Journal of Nuclear Materials 378 (2008) 120–125

Contents lists available at ScienceDirect

Journal of Nuclear Materials

journal homepage: www.elsevier.com/locate/jnucmat

An elastoplastic phase-field model for the evolution of hydride precipitation in zirconium. Part II: Specimen with flaws

X.H. Guo [a,b], S.Q. Shi [a,*], Q.M. Zhang [b], X.Q. Ma [c]

[a] Department of Mechanical Engineering, The Hong Kong Polytechnic University, Hung Hom, Kowloon, Hong Kong
[b] State Key Laboratory of Explosion and Safety Science, Beijing Institute of Technology, Beijing 100081, China
[c] Department of Physics, University of Science and Technology Beijing, Beijing 100083, China

ARTICLE INFO

Article history:
Received 1 February 2008
Accepted 16 May 2008

ABSTRACT

An elastoplastic phase-field model, described in Part I, was applied to bulk materials containing flaws such as sharp cracks and blunt notches. An additional set of long range order parameters, namely, stress-free strains for flaws, was introduced. The nucleation and growth of hydrides near a void or a crack were simulated by the proposed elastoplastic phase-field model. The effects of notch root radius, hydrogen concentration in solid solution, yield stress of the matrix and the level of externally applied stress on hydride morphology around flaws were studied. It is demonstrated that parameters such as the distribution of the tensile stress component perpendicular to the hydride platelet normal may be closely monitored during hydride growth near a flaw with or without externally applied stresses. Combined with a fracture criterion and real experimental data, the model is capable of predicting the rate and morphology of hydride precipitation, and crack initiation near flaws.

1. Introduction

A majority of metals in the chemical periodic table can form metal hydrides under different conditions. The presence of hydrides in metals may lead to a process of slow crack propagation called delayed hydride cracking (DHC) [1–3]. In DHC, hydrogen atoms in solid solution diffuse to high tensile stress regions such as crack tips, and form hydrides if the concentration of hydrogen is high enough. The hydrides at flaws may fracture under suitable conditions and the crack will advance. Then the process of DHC will repeat itself again. Modeling of DHC is challenging, not only because it involves three distinct phenomena, i.e., hydrogen diffusion, hydride phase transformation and fracture, but also because in realistic situations, it depends on factors such as materials geometry, hydrogen content, thermal and mechanical history, and microstructure. The theoretical framework developed in Part I of this study [4] makes it possible to include all these phenomena and factors into consideration. In the past, theoretical modeling and experimental study of DHC initiation were usually done separately for three types of initiation sites, (i) a sharp crack; (ii) a blunt notch, and (iii) a nominally smooth surface. Criteria for DHC initiation at these three sites were different. For a sharp crack, a critical threshold stress intensity factor had been used [5], while for a blunt notch or a smooth surface, either the maximum tensile stress at the notch [6] or a remotely applied tensile stress was used, respectively. With the proposed elastoplastic phase-field model, it is feasible to study and predict DHC initiation under one theoretical framework. No matter whether the fracture criterion is a critical stress intensity factor, or a critical stress component, or a critical displacement, or a critical strain component, or a critical energy release rate, the proposed elastoplastic phase-field model can handle all these parameters with ease because most of these parameters are actually evaluated for any location at every time step within the concerned specimen during the theoretical calculation. Since DHC initiation at sharp cracks and blunt notches are, by far, the most important in safety assessment, the Part II of this study will focus on these two cases.

2. The elastoplastic phase-field model for specimens with flaws

The theoretical framework developed in Part I for smooth specimens without flaws is not adequate for specimens with flaws such as voids, notches and cracks. Special treatments for regions of flaws are required. It has been demonstrated [7] that an equivalent description can be made of the strain energy of an anisotropic discontinuous body with cracks under applied stress by an anisotropic continuous noncracked body of the same macroscopic size and shape, but with additional heterogeneous misfit stress-free strains inside the flaws. Denoting such additional stress-free strains as $\varepsilon_{ij}^{\mathrm{def}}(\mathbf{r}, t)$, one can re-write the total eigenstrain of the system as

* Corresponding author. Tel.: +852 2766 7821; fax: +852 2365 4703.
E-mail address: mmsqshi@polyu.edu.hk (S.Q. Shi).

0022-3115/$ - see front matter © 2008 Elsevier B.V. All rights reserved.
doi:10.1016/j.jnucmat.2008.05.006

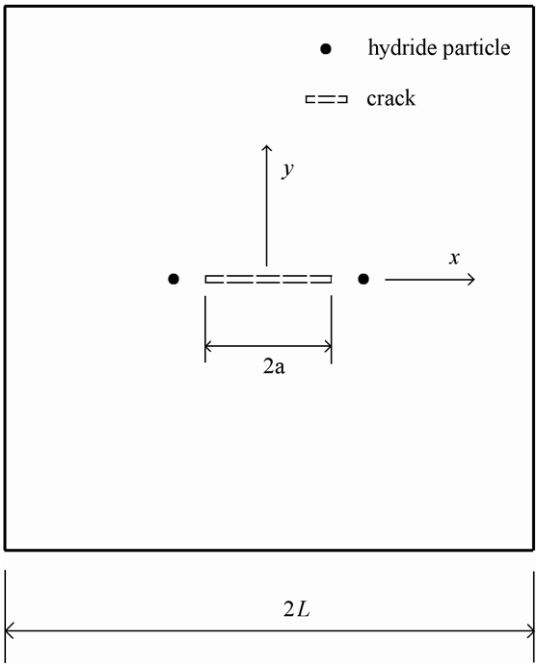

Fig. 1. A schematics for two circular hydride nuclei near to the tips of a central crack.

$$\varepsilon_{ij}^{0}(\mathbf{r}) = \sum_{p=1}^{v} \varepsilon_{ij}^{\eta_p}(p)\eta_p^2(\mathbf{r}) + \varepsilon_{ij}^{c}\delta c(\mathbf{r}) + \varepsilon_{ij}^{p}(\mathbf{r}) \quad \text{(outside flaws)} \tag{1a}$$

$$\varepsilon_{ij}^{0}(\mathbf{r}) = \varepsilon_{ij}^{\mathrm{def}}(\mathbf{r}) \quad \text{(inside flaws)} \tag{1b}$$

The meanings of each term in (1a) were given in Part I. Since $\sigma_{ij}(r,t) = -\frac{\partial E}{\partial \varepsilon_{ij}^{0}(r,t)}$ where E is the total strain energy of the system, we want to make sure that at the equilibrium state, stress components inside flaws vanish. In other words, the following set of dynamic equations must be valid,

$$\frac{\partial \varepsilon_{ij}^{\mathrm{def}}(\mathbf{r},t)}{\partial t} = -K_{ijkl}\frac{\delta E}{\delta \varepsilon_{kl}^{\mathrm{def}}(\mathbf{r},t)} \quad \text{(inside flaws)} \tag{2}$$

where K_{ijkl} is a kinetic coefficient which has no physical meaning. In general, the total stress $\sigma_{ij}(r,t)$ is nonzero outside the voids and cracks, but it vanishes inside them. Therefore, at the equilibrium state, the flaw domains containing the misfit strains $\varepsilon_{ij}^{\mathrm{def}}(\mathbf{r},t)$ can be removed from the body without disturbing the strain and stress distributions outside the domains.

The Eq. (2) shall be solved together with the other three sets of dynamic equations given in Part I, namely,

$$\frac{\partial \eta_p(\mathbf{r},t)}{\partial t} = -L_p\frac{\delta F}{\delta \eta_p(\mathbf{r},t)} + \zeta_p(\mathrm{r},t) \tag{3}$$

$$\frac{\partial c(\mathbf{r},t)}{\partial t} = M\nabla^2\frac{\delta F}{\delta c(\mathbf{r},t)} + \xi(\mathrm{r},t) \tag{4}$$

$$\text{and} \quad \frac{\partial \varepsilon_{ij}^{p}(\mathbf{r}_p,t)}{\partial t} = -N_{ijkl}\frac{\delta E^{\mathrm{dis}}}{\delta \varepsilon_{kl}^{p}(\mathbf{r}_p,t)} \tag{5}$$

Not like the Eq. (2), Eqs. (3)–(5) are valid only outside of flaws. If a fracture criterion of hydrides is given, the theoretical framework described above is able to predict DHC initiation at flaws. In stead of Eq. (2), our early work had used a separate stress calculation from another numerical package such as finite element method [8]. The current work described in Part I and Part II does not require a separate solution. The stress/strain field was solved through Eqs. (2) and (5) simultaneously with the phase-field Eqs.

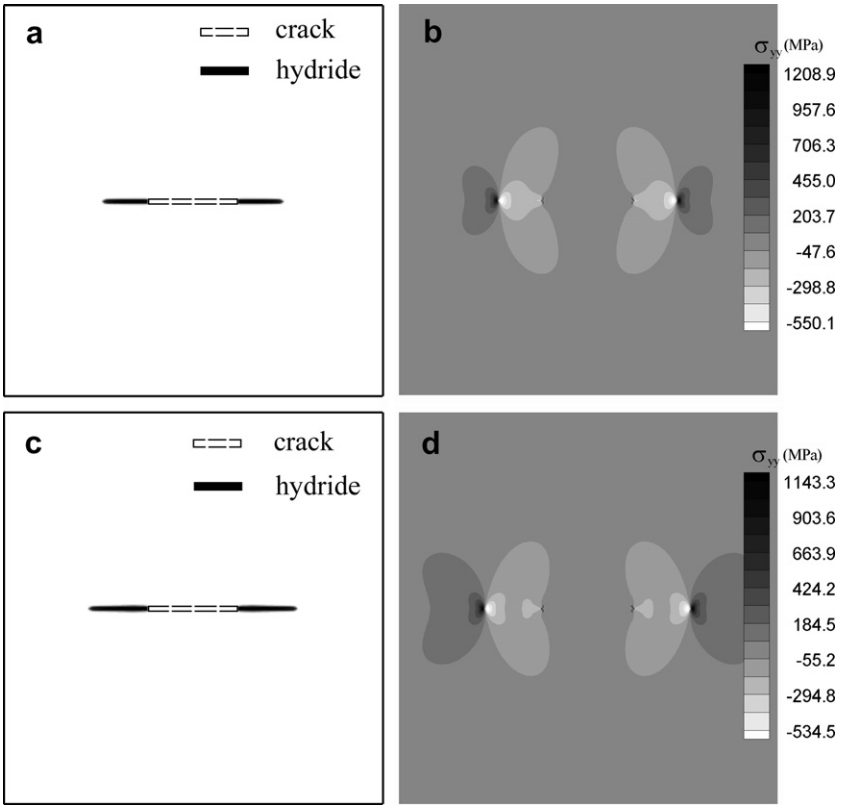

Fig. 2. The growth of hydride particles in elastic matrix and stress distribution around a central crack without externally applied stress: (a) hydride shape at $t^* = 5000$; (b) σ_{yy} at $t^* = 5000$; (c) hydride shape at $t^* = 8000$; (d) σ_{yy} at $t^* = 8000$.

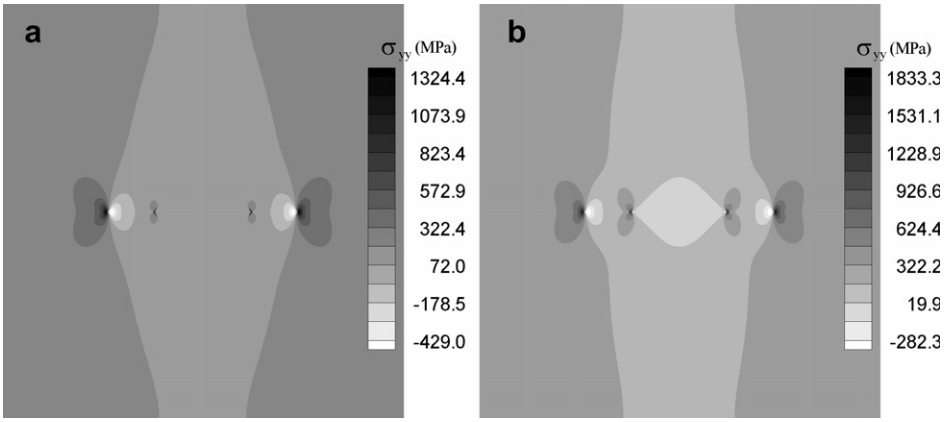

Fig. 3. The stress distribution of σ_{yy} under externally applied stress: (a) $\sigma^{appl} = 100$ MPa; (b) $\sigma^{appl} = 200$ MPa.

(3) and (4) at each time increment. In fact, the total strain energy E in Eq. (2) includes all the eigenstrains such as those for hydrides and hydrogen interstitials. Therefore, the volume expansions by hydride formation and hydrogen interstitials were automatically taken into account, and the stress/strain redistribution due to hydride formation and hydrogen interstitials were fully realized at every time step.

It should be noted that we had solved Eqs. (2) and (5) together to predict the plastic zone size and shape around a circular hole or a sharp crack at equilibrium condition [9]. An excellent agreement was obtained when compared with a finite element calculation.

3. Simulation results and discussion

The thermodynamic and mechanical parameters used in Part I (such as A_1–A_7, elastic constants, yield stress, Poisson's ratio and so on) will be applied for specimens with flaws. If the temperature is not kept at a constant level, the temperature dependence of these parameters should be defined.

In the following simulations, a central hole or a central crack in a 2-D specimen was chosen for analysis. This is due to the numerical method (the semi-implicit Fourier-spectral algorithms) used for solving dynamic equations. This numerical method can significantly reduce the computation time by orders of magnitude with excellent accuracy, but it requires periodic boundary conditions. When the size of the central crack is small compared to the size of the specimen, the difference in numerical solutions between a half sided central crack and an edge crack on a free surface will be small. One can use different numerical methods (such as [10,11]) with more realistic boundary conditions, but the computational efficiency will be reduced significantly. At this stage, our main task is to verify the soundness of the theoretical framework.

We first assume that the zirconium matrix can only deform elastically and that the externally applied stress is zero. In order to investigate the interaction between a hydride and a crack, two hydride nuclei were embedded near the two tips of a central crack and allowed them to grow horizontally, as shown in Fig. 1. After 5000 time steps of hydride growth, the two nuclei evolved into plate-like particles, and one end of the each hydride particle contacted with the crack tip, see Fig. 2(a). The distribution of the stress component σ_{yy} at this moment is shown in Fig. 2(b). If the simulation is continued, these hydrides will grow longer in the direction far away from the crack. Fig. 2(c) and (d) shows the size of hydrides and stress σ_{yy} at 8000 time steps, respectively. Because the external stress was not applied, the stress σ_{yy} inside hydrides is compressive and a less compressive for a longer hydride. If we stop the hydride growth at 5000 time steps and apply the external stress to 100 or 200 MPa, as seen in Fig. 3, the stress σ_{yy} inside the hydrides near crack tips become less compressive (Fig. 3(a)) and even tensile (Fig. 3(b)), meaning that the hydrides become vulnerable to fracture. Fig. 4 shows the distribution of σ_{yy} along the crack plane with or without externally applied stresses. One can see that the stress inside the hydride increased significantly due to the externally applied stress. Under the assumption of pure elastic deformation, the brittle hydrides should be broken at crack tips under such a high tensile stress.

From Fig. 4, one can also find that the stress σ_{yy} in the metal matrix was very high close to the hydride tips, therefore, plastic deformation would occur in these regions. Based on the proposed elastoplastic phase-field model given in Section 2, we repeated the simulations presented earlier, and the growth of hydride particles and stress redistribution are shown in Figs. 5–7 at 7000 time steps. As being expected, the plastic zones emerged around the ends of plate-like hydride particles when the external stress was not applied. Due to the plastic deformation, the peak stress inside and outside of the hydrides was decreased significantly. However, if the external stress was applied, the stress in hydride particles near the crack tip became tensile, see Fig. 7 curves *b* and *c*. It reached as high as 840 MPa when the externally applied stress was increased to 200 MPa. Depending on the fracture criterion to be used, such a high tensile stress may or may not cause crack initiation at these crack-tip hydrides.

The above simulations were done by placing hydride nuclei at specific locations near a crack. One can also investigate the

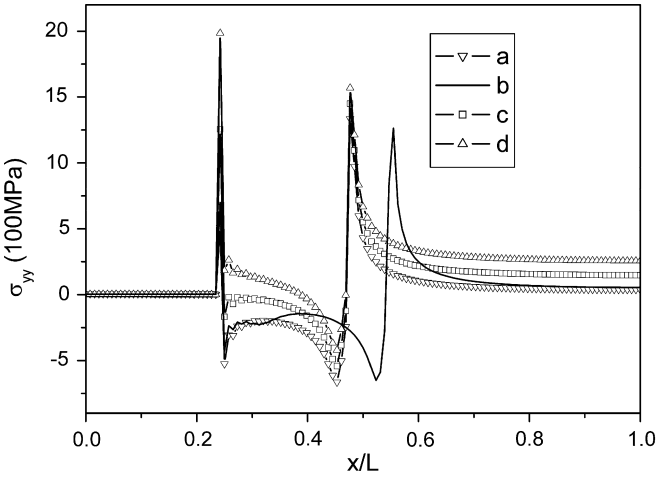

Fig. 4. Variation of stress σ_{yy} along horizontal midline: (a) $t^* = 5000$ and (b) $t^* = 8000$ without external stress applied; under an external applied stress of (c) $\sigma^{appl} = 100$ MPa and (d) $\sigma^{appl} = 200$ MPa for $t^* = 5000$.

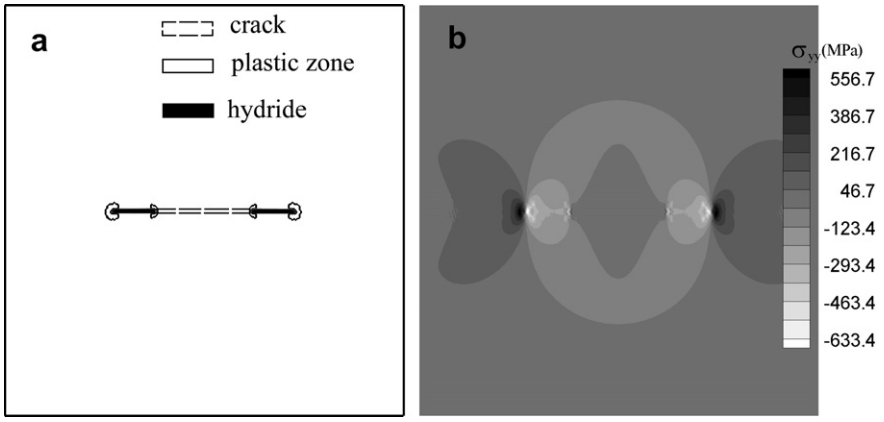

Fig. 5. Without externally applied stress, (a) the plastic zone and (b) σ_{yy} resulted from the growth of hydride particles in elastoplastic matrix near to a central crack.

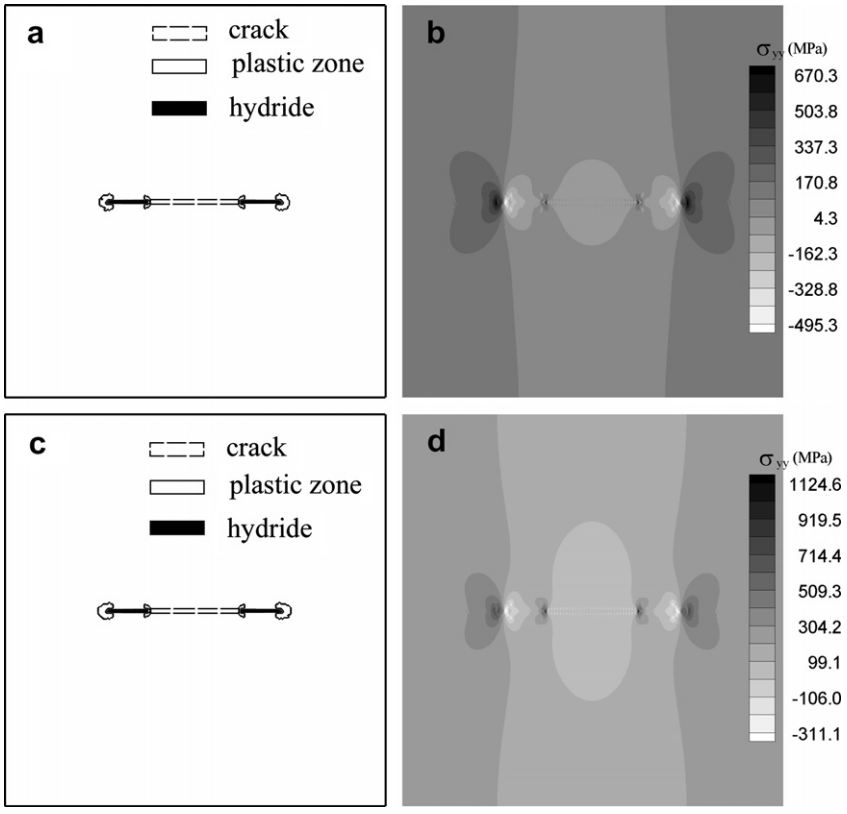

Fig. 6. Under an external stress of $\sigma^{appl} = 100$ MPa: (a) the plastic zone and (b) σ_{yy} around the two hydride particles; under $\sigma^{appl} = 200$ MPa: (c) the plastic zone and (d) σ_{yy} around the two hydride particles.

arbitrary nucleation and growth of hydride particles round a crack or notch under externally applied stresses. To mimic a randomly oriented polycrystalline zirconium with a fine grain structure, we assume that the hydride platelets can grow along any direction. A 2-D model with a central U-shaped hole is schematically shown in Fig. 8. The length of the hole was $L = 200$ grids, the initial hydrogen concentration was set as $c_0 = 0.01$, and a yield stress of 800 MPa for the matrix was applied. The effect of root radius of the hole was investigated by comparing three numerical simulations at three different notch radii, i.e., $R = 50$, 25, and 2 grids, respectively. It should be mentioned that a real dimension of each grid can be defined if all phenomenological parameters such as diffusion coefficient were given. An example of phase-field simulations with real dimensions for hydrogen embrittlement was reported recently in [12], which was very time-consuming in computation. In the current analysis, the externally applied stresses (σ^{appl}) for three different notches were selected in such a way that the maximum stress at notch tips was about 950 MPa before hydride precipitation started. The morphologies of hydride precipitation around these notches after 8000 time steps are shown in Fig. 9. It is clear that for the same peak tensile stress, same hydrogen concentration in solid solution and same period of diffusion time, the sharper the notch root radius is, the more focused hydride precipitation would occur. In this situation, the amount of hydride precipitation is dependent on the size of the area where a high tensile stress is maintained. Hydride platelets were growing normal to the notch root surfaces. The intention of Fig. 9 was to compare the morphology of hydrides as a function of notch

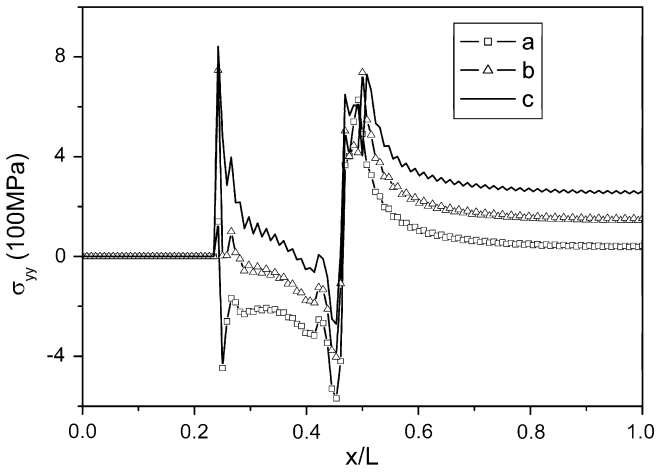

Fig. 7. The variation of σ_{yy} along horizontal midline: (a) $\sigma^{appl} = 0$ MPa; (b) $\sigma^{appl} = 100$ MPa and (c) $\sigma^{appl} = 200$ MPa.

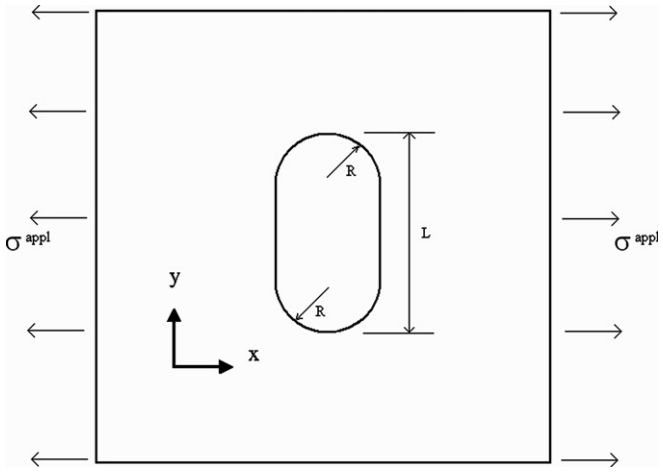

Fig. 8. Schematic configuration of a 2-D model with a central hole subjected to an externally applied stress σ^{appl}.

geometry. In the current case, initial hydrogen concentration in solution, yield stress and peak stresses were fixed (same for all notch geometry). Another way to check the hydride morphology as a function of notch geometry is to fix the applied stress in simulations, and then the peak stresses will be vastly different, which will mixes up the effects of geometry and peak stress as the peak stress could be important for crack initiation.

In another set of numerical simulations, the root radii of notches were fixed at $R = 50$, and the externally applied stress was set to 200 MPa, while the initial hydrogen concentration in solid solution was selected to be $c_0 = 0.1$, 0.01 and 0.001, respectively. The simulation results of hydride precipitation are shown in Fig. 10. With the decrease in hydrogen concentration, the hydride precipitation became more and more difficult, resulting in a decrease in the amount of hydrides precipitation.

We now focus our study on hydrides near a crack tip. As shown in Fig. 11, a central crack with the dimensions of 100 grids in length and 4 grids in width was introduced and subjected to a horizontally applied stress of $\sigma^{appl} = 200$ MPa. To increase the effect of plastic deformation, we assumed that the yield stress of zirconium matrix was 540 MPa to mimic the unirridiated materials. The initial hydrogen concentration was set to be $c_0 = 0.1$ at%. This concentration is artificially high for the purpose of demonstrating the capability of the model from a low density of hydrides to a very high density of hydrides. Simulations with a low initial hydrogen concentration can be easily done, while a little variation in hydride density as a function of time will be seen. The morphology of hydride precipitation was recorded after 5000, 10,000 and 25,000 time steps, respectively, see Fig. 11. Although the hydrides grow almost in the whole field, they are inclined to nucleate and grow in the regions near the crack tips. Comparing with Fig. 10, we can see that the evolution rate of hydrides was lower if the yield stress of zirconium matrix decreases. Moreover, most hydrides are perpendicular to the applied tensile stress. The model can monitor stress, strain and other parameters at any location and at any time. Fig. 12 gives an example of the distribution of the stress σ_{xx} in a crack-tip hydride. This hydride was indicated in Fig. 11 by letters I, II, and III for three different moments in time. Due to the complicated hydride morphologies and the interactions among hydrides, the stress component σ_{xx} inside this hydride fluctuated. In the early stage of growth, a few hydrides grew near the crack tip, and the length of the hydrides was small. This hydride was subjected to low tensile stress, even compressive stress, Fig. 12(a). When the hydride grew longer, the average tensile stress inside this hydride increased, see Fig. 12(b) and (c), which may result in crack initiation at some location inside the hydride.

4. Conclusion

A general elastoplastic phase-field model was used to simulate the nucleation and growth of hydride precipitates near a flaw in zirconium. The effects of notch root radius, hydrogen concentration in solid solution, yield stress of the matrix and the level of externally applied stress on hydride morphology around flaws were studied. It is demonstrated that parameters such as the distribution of the tensile stress component perpendicular to the

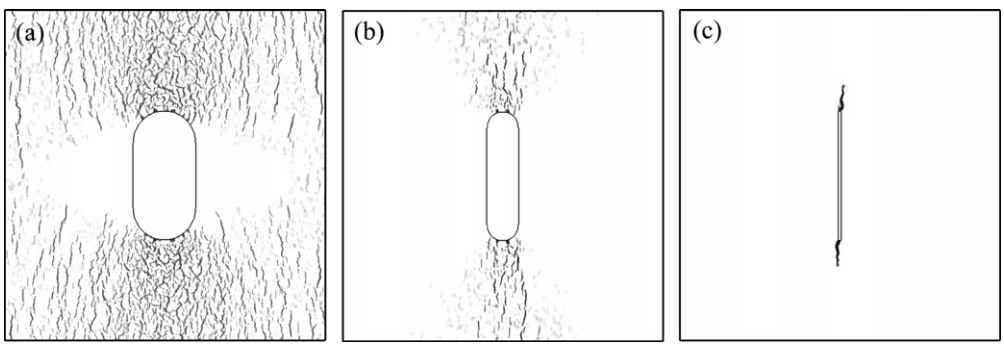

Fig. 9. Hydride precipitation around a hole under an external stress applied horizontally. (a) $R = 50$; (b) $R = 25$; (c) $R = 2$. $c_0 = 0.01$, yield stress = 800 MPa, and maximum tensile stress at all notch tips = 950 MPa before hydride precipitation.

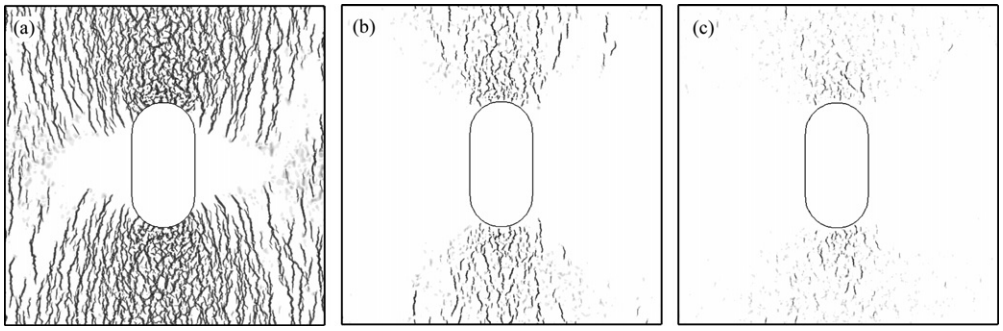

Fig. 10. Hydride precipitation around a hole when $R = 50$, $\sigma^{appl} = 200$ MPa, yield stress = 800 MPa, and $t^* = 9000$. (a) $c_0 = 0.1$; (b) $c_0 = 0.01$; (c) $c_0 = 0.001$.

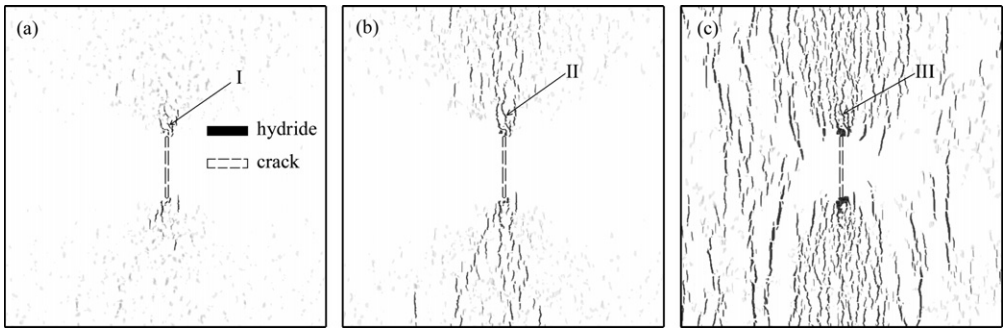

Fig. 11. The morphologies of hydride precipitation around a crack subjected to an external stress $\sigma^{appl} = 200$ MPa; $c_0 = 0.1$; yield stress = 540 MPa. (a) $t^* = 5000$; (b) $t^* = 10,000$; (c) $t^* = 25,000$.

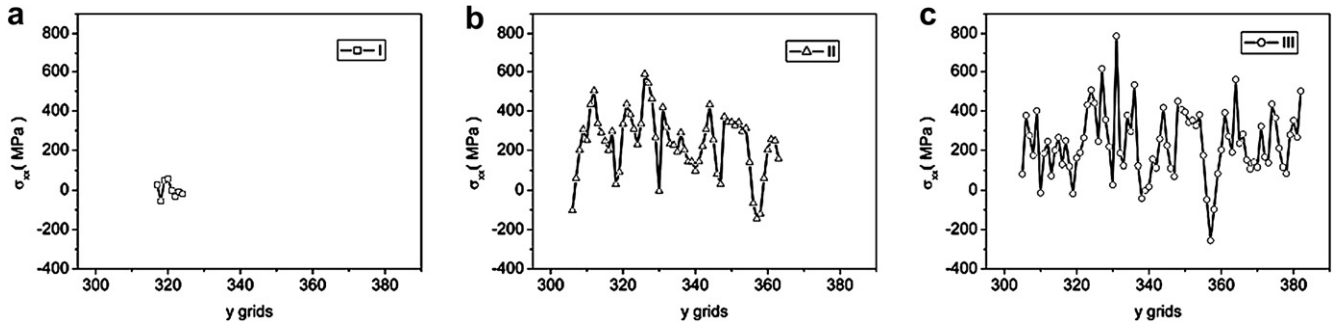

Fig. 12. The distribution of σ_{xx} along the hydride indicated by I, II and III in Fig. 11.

hydride platelet normal may be closely monitored during hydride growth near a flaw with or without externally applied stresses. The results of the simulations are consistent with the general experimental observations. Combined with a fracture criterion and real experimental data (such as diffusion coefficient), the model is capable of predicting the rate and morphology of hydride precipitation, and crack initiation near flaws.

Acknowledgements

This work was supported by a research grants from the Research Grants Council of Hong Kong (PolyU 5265/06E) for Shi, and from the National Natural Science Foundation of China (#10702007) for Guo.

References

[1] D.N. Williams, J. Inst. Met. 91 (1962) 147.
[2] R. Dutton, K. Nuttall, M.P. Puls, L.A. Simpson, Metall. Trans. A 8 (1977) 1553.
[3] N. Winzer, A. Atrens, W. Dietzel, G. Song, K.U. Kainer, Mater. Sci. Eng. A 466 (2007) 18.
[4] X.H. Guo, S.Q. Shi, Q.M. Zhang, X.Q. Ma, Part I of this Study, J. Nucl. Mater. 378 (2008) 110.
[5] S.Q. Shi, M.P. Puls, J. Nucl. Mater. 208 (1994) 232.
[6] S.Q. Shi, M.P. Puls, S. Sagat, J. Nucl. Mater. 208 (1994) 243.
[7] A.G. Khachaturyan, Theory of Structural Transformations in Solids, Wiley, New York, 1983.
[8] X.Q. Ma, S.Q. Shi, C.H. Woo, L.Q. Chen, Mech. Mater. 38 (2006) 3.
[9] X.H. Guo, S.Q. Shi, X.Q. Ma, Appl. Phys. Lett. 87 (2005) 221910.
[10] N. Provatas, J. Dantzig, N. Goldenfeld, J. Comp. Phys. 148 (1999) 265.
[11] D. Schrade, R. Mueller, B.X. Xu, D. Gross, Comput. Meth. Appl. Mech. Eng. 196 (2007) 4365.
[12] X.H. Guo, S.Q. Shi, L.J. Qiao, J. Am. Ceram. Soc. 90 (2007) 2868.